

# Optical monitoring of the $z=4.40$ quasar Q 2203+292

E. P. Ovcharov<sup>1\*</sup>, P. L. Nedialkov<sup>1</sup>, A. T. Valcheva<sup>4</sup>, V. D. Ivanov<sup>3</sup>,  
N. A. Tikhonov<sup>2</sup>, I. S. Stanev<sup>1</sup>, A. B. Kostov<sup>4</sup> and Ts. B. Georgiev<sup>4</sup>

<sup>1</sup>*Department of Astronomy, University of Sofia, 5 James Bourchier, Sofia 1164, Bulgaria*

<sup>2</sup>*Special Astrophysical Observatory, Russian Academy of Sciences, N. Arkhyz, KChR 369167, Russia*

<sup>3</sup>*European Southern Observatory, Ave. Alonso de Cordova 3107, Casilla 19, Santiago 19001, Chile*

<sup>4</sup>*Institute of Astronomy, Sofia 1784, Bulgaria*

2 February 2022

## ABSTRACT

We report Cousins  $R$ -band monitoring of the high-redshift ( $z=4.40$ ) radio quiet quasar Q 2203+292 from May 1999 to October 2007. The quasar shows maximum peak-to-peak light curve amplitude of  $\sim 0.3$  mag during the time of our monitoring, and  $\sim 0.9$  mag when combined with older literature data. The rms of a fit to the light curve with a constant is 0.08 mag and 0.2 mag, respectively. The detected changes are at  $\sim 3$ -sigma level. The quasar was in a stable state during the recent years and it might have undergone a brightening event in the past. The structure function analysis concluded that the object shows variability properties similar to those of the lower redshift quasars. We set a lower limit to the Q 2203+292 broad line region mass of  $0.3\text{--}0.4 M_{\odot}$ . Narrow-band imaging search for redshifted Ly $\alpha$  from other emission line objects at the same redshift shows no emission line objects in the quasar vicinity.

**Key words:** quasar: general - quasars: individual: Q 2203+292

## 1 INTRODUCTION

Many quasars show short-term or/and long-term variability (Ulrich, Maraschi & Urry 1997). These changes in the source flux help to constrain the physics and the size of the central engine. Astronomers came to an early understanding that the central engines of the AGNs and QSOs can not be resolved easily, if at all, but that the variability timescales measure the size of the emitting regions (i.e. Blandford & McKee 1982). Later on, this became the basis of reverberation studies (for a recent review see Peterson et al. 2004 and the references therein) that could map the innermost broad line regions (hereafter BLR). Nevertheless, the exact variability mechanisms remain unclear.

Typically, the variability is aperiodic, but it does show some dependencies on time lag, luminosity, wavelengths and redshift. For example, the variability amplitude increases with time lag (Vanden Berk et al. 2004), more luminous quasars are less variable (Vanden Berk et al. 2004; de Vries et al. 2005; Giveon et al. 1999), and the variability increases toward the blue part of the spectrum (Vanden Berk et al. 2004; de Vries et al. 2005). It is particularly difficult to constrain the variability versus redshift dependence because of the inevitable biases at high redshift, limiting the quasar lu-

minosity range, the probed time-baseline, etc. of the more distant quasars.

The radio properties of QSOs also seem to be related to the optical variability: the radio-loud ones are relatively more variable than the radio quiet ones, and the blazars show even stronger variability because of beaming, which is quite different than the long-term variability studied in this work. For a more comprehensive review of the QSO variability properties we refer the reader to the summary of Wold, Brotherton & Shang (2007). As of now, there is no commonly accepted theory of the QSO variability and the existence of some strange objects, albeit rare ones, complicates the picture even further. A good example is the radio-quiet QSO SDSS J153259.96-003944.1 (Stalin & Sri-anand 2005) who is the prototype of the rare class of weak (or absent) emission-line quasars (WLQs). This object shows strong long-term variability and flat optical spectrum like BL Lacs but there is no radio emission, no optical polarization and no X-ray (Shemmer et al. 2006). These properties may be explained by a deficit of line-emitting gas in the vicinity of the central continuum source, similar to the X-ray weak quasar PHL 1811 (Leighly et al. 2007 and the references therein).

The most comprehensive quasar variability studies, especially the ones covering long time scales, are focused either on bright low-redshift ones (Hook et al. 1994; Hawkins

\* E-mail: evgeni@phys.uni-sofia.bg

**Table 1.** Broad band photometry of Q 2203+292 since 1987.

Date yyyy/mm/dd	Reference	Filter	Brightness mag
1987/09/25	McCarthy et al. (1988)	$r_s$	$20.78 \pm 0.09$
		$V$	$22.0 \pm 0.3$
		$I$	$21.1 \pm 0.3$
1988/09/12	Schneider, Schmidt & Gunn (1989)	$r_4$	$20.88 \pm 0.05$
		$g_4$	$22.33 \pm 0.06$
1989/09/09	Crampton et al. (1992)	$R_C$	$20.7 \pm 0.1$
		$V$	$22.0 \pm 0.1$
1990/06/21	Crampton (private communication)	$R_C$	$20.4 \pm 0.1$

2002), or they study the behavior of the structure function for large samples (de Vries, Becker & White 2003; de Vries et al. 2005; Hovatta et al. 2007). The literature is lacking well sampled light curves of individual distant quasars, with the notable exception of Kaspi et al. (2007) with whom we share five objects from our extended program. While challenging, the distant QSOs are also rewarding because the variability can help constrain the size of the QSO accretion disks (Hawkins 2007) at early times. Furthermore, identifying variable high-redshift quasars is a necessary first step for reverberation mapping of their broad line regions (i.e. Kaspi et al. 2007). These arguments motivated us to start an optical monitoring study of QSOs with  $z \geq 4$ .

Here we present a photometric sequence for Q 2203+292, which is one of the first detected quasars within that redshift range (Dickinson & McCarthy 1987) and it is radio-quiet (Schneider et al. 1992; Schmidt et al. 1995; Omont et al. 1996). Surdej et al. (1993), Crampton, McClure & Fletcher (1992) and Kochanek (1993) reported that it is not gravitationally lensed. The only study in the literature on the Q 2203+292 variability comes from McCarthy et al. (1988) who concluded from three Lick 3m plates and two plates from the 5m Hale telescope (Longair & Gunn 1975; Riley, Longair & Gunn 1980) that the quasar did not vary strongly over a period of the 15 years since its discovery. A few additional broadband observations of Q 2203+292 are reported elsewhere, but they are in different photometric systems (see Table 1).

Turner (1991) calculated for Q 2203+292 a mass of the central black hole of  $(0.69-9.6) \times 10^8 M_\odot$  and a mass accretion rate of  $1.6-22 M_\odot/\text{yr}$ , depending on the adopted cosmological model. These values are typical for the quasars at the same redshift (Turner 1991; Dietrich & Hamann 2004).

## 2 OBSERVATIONS AND DATA REDUCTION

### 2.1 Observing Strategy and Basic Data Reduction

We monitored Q 2203+292 in  $R$ -band with a variety of instruments and telescopes. ESO Archive images were also used. The observing log is shown in Table 2. Typically, the total integration time was split into a few separate frames (as listed in the last column) and the telescope was jittered by a few arcsec between each of them to remove the artifacts

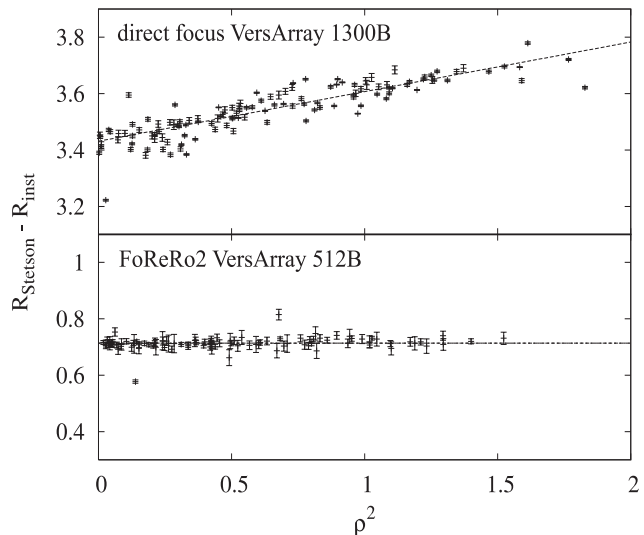


**Figure 1.** Radial flux variation. The difference  $R_{Stetson} - R_{inst}$  magnitudes for all detectable stars in the field of the globular clusters NGC 7790 and NGC 2420, taken with VersArray 1300B in direct focus (top) and VersArray 512B in red channel of FoReRo2 (bottom) versus the squared normalized distance from the center of the detector  $\rho^2$ .

caused by the detector’s cosmetic defects. All observations were performed in clear, photometric nights. The object was monitored during culmination, whenever possible, to minimize the airmass variation during the observations.

The basic data reduction includes: bias subtraction, flat fielding, alignment of individual frames and combination. We used the standard IRAF<sup>1</sup> routines to perform them.

### 2.2 Instrumental Magnitudes and Corrections for Systematical Effects

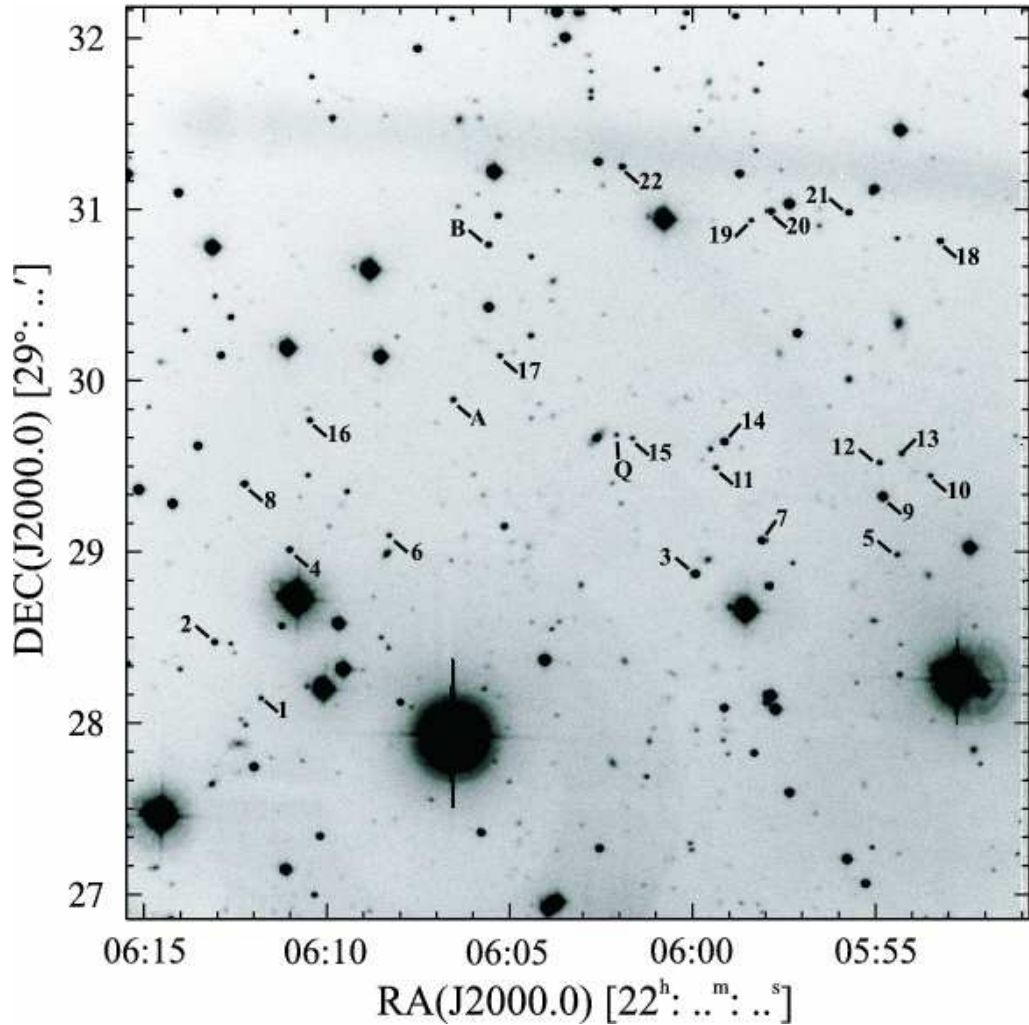
We carried out aperture photometry on the combined images. The aperture diameter was set to the size of the FWHM to optimize the signal-to-noise, because the sky contributed comparable flux to the target flux in the wings of the image. This is possible because: (i) the QSO PSF is indistinguishable from the PSF profiles of the stars, and (ii) the PSF variations across the field of view are negligible. Therefore, the selection of the aperture does not have an effect on the relative photometry we obtained on each individual image. Next, the zero points we determined by comparing the instrumental and the standard magnitudes of the calibration field (measured the same way) contain into themselves the aperture corrections. For more details on the photometric calibration see Sec. 2.3.

The Photometrics AT200A and the VersArray 1300B cameras exhibit spatial flux variations (Fig. 1). They were

<sup>1</sup> IRAF is the Image Reduction Analysis and Facility made available to the astronomical community by the National Optical Astronomy Observatories, which are operated by AURA, Inc., under contract with the U.S. National Science Foundation. STSDAS is distributed by the Space Telescope Science Institute, which is operated by the Association of Universities for Research in Astronomy (AURA), Inc., under NASA contract NAS5-26555.

**Table 2.** Observing log.

Data yyyy/mm/dd	Instrument@Telescope@Site	Pixel Scale [arcsec px <sup>-1</sup> ]	FoV [arcmin <sup>2</sup> ]	Airmass	FWHM [arcsec]	Total Integration Time [s]
1999/05/15	FORS1@VLT@Paranal	0.25	6.8×6.8	1.76	0.4	1×100=100
2003/08/26	Photometrics AT200A@2m@Rozhen	0.29	5.0×5.0	1.04	1.1	3×1200=3600
2004/10/09	Photometrics AT200A@2m@Rozhen	0.29	5.0×5.0	1.03	1.4	3×1200=3600
2005/10/01	EEV/Marconi 42-40@1m@SAO	0.27	4.6×4.6	1.23	1.2	3×200=600
2005/11/04	VersArray 1300B@2m@Rozhen	0.26	5.7×5.5	1.11	1.8	9×300=2700
2005/11/06	VersArray 1300B@2m@Rozhen	0.26	5.7×5.5	1.07	2.0	6×600=3600
2006/06/29	Photometrics AT200A@2m@Rozhen	0.29	5.0×5.0	1.54	1.6	10×180+2×300=2400
2006/08/18	Photometrics AT200A@2m@Rozhen	0.29	5.0×5.0	1.04	1.4	3×1200=3600
2006/08/19	Photometrics AT200A@2m@Rozhen	0.29	5.0×5.0	1.02	1.4	2×1200=2400
2006/08/25	FoReRo2@2m@Rozhen	0.82	7.0×7.0	1.32	2.4	8×300=2400
2006/10/23	EEV/Marconi 42-40@1m@SAO	0.27	4.6×4.6	1.04	1.1	3×300=900
2006/10/24	EEV/Marconi 42-40@1m@SAO	0.27	4.6×4.6	1.09	1.0	3×300=900
2007/09/10	VersArray 1300B@2m@Rozhen	0.26	5.7×5.5	1.14	1.5	2×1200=2400
2007/10/04	VersArray 1300B@2m@Rozhen	0.26	5.7×5.5	1.04	1.0	3×1200=3600

**Figure 3.** Identification chart with standard stars in the field of Q 2203+292. The image was obtained with 2m RCC telescope of NAO, Rozhen on 2004 October 9. The field of view is 5×5 arcmin<sup>2</sup>. North is up, and East is to the left.

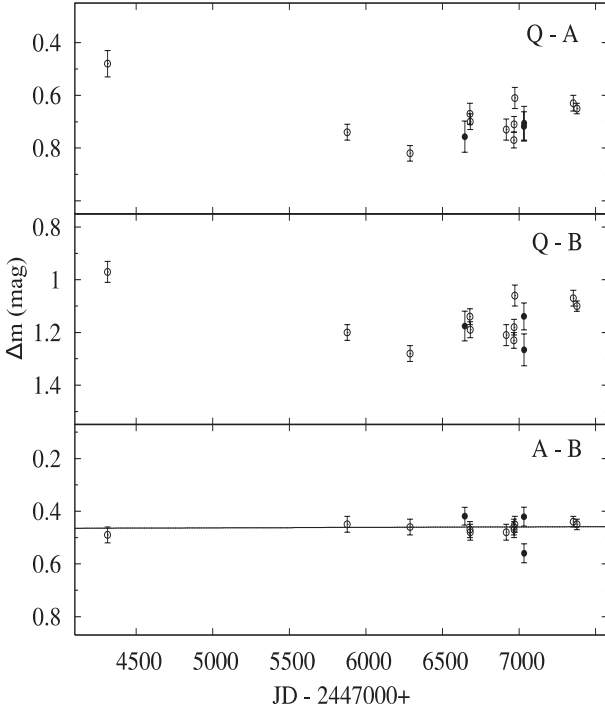


**Figure 2.** Difference between the magnitudes of the quasar Q 2203+292 and the reference stars A and B is shown on the top and middle panels. The difference between A and B reference stars is shown on the bottom panel. The solid line is the linear fit to the data. The first open circle indicates the VLT data and the other open circles are Rozhen Observatory data. The solid circles are the data from the 1m SAO telescope.

removed as described in Markov (2005), correcting the instrumental magnitudes as follows:

$$R = c_\rho \rho^2 + R_{inst}, \quad (1)$$

where  $c_\rho$  is a known coefficient (0.12 for Photometrics AT200A and 0.17 for VersArray 1300B) and  $\rho$  is the distance from the center of the detector. This is normalized by the detector half-size, and it varies from 0 to  $\sqrt{2}$ :

$$\rho = \sqrt{\left(1 - \frac{x}{x_c}\right)^2 + \left(1 - \frac{y}{y_c}\right)^2}. \quad (2)$$

Here  $x$  and  $y$  are the coordinates of the object in pixels and  $x_c$  and  $y_c$  are the coordinates of the central pixel. Note that for the purpose of our differential photometry this correction is minor, because the quasar and the comparison stars were placed at the same position, within the pointing errors, so  $\Delta\rho^2 < 0.1$ , translates into 0.02 mag extra uncertainty in the differential magnitudes Q-A and Q-B (see Fig. 2). An additional source of error, albeit also small, is the jittering between the individual frames, that comprise the individual epochs of our light curve. It was always 3-4 arcsec (except 12 arcsec in one case) which corresponds to ignorable magnitude error. Interestingly, the FoReRo2 (Jockers et al. 2000) shows no spatial effects, as verified from observations of Stetson standards (Stetson 2000) taken during a few different photometric nights.

Differential light curves of the quasar were generated relative to two nearby comparison stars imaged on the same

**Table 3.** Differential instrumental magnitudes between the quasar and the comparison stars A ( $\alpha_{2000}=22:06:07.15$ ,  $\delta_{2000}=29:30:12.9$ ) and B ( $\alpha_{2000}=22:06:06.33$ ,  $\delta_{2000}=29:31:08.0$ ) and between the two comparison stars.

Date yyyy/mm/dd	Q-A [mag]	Q-B [mag]	A-B [mag]
1999/05/15	$0.48 \pm 0.05$	$0.97 \pm 0.04$	$0.49 \pm 0.03$
2003/08/26	$0.74 \pm 0.03$	$1.20 \pm 0.03$	$0.45 \pm 0.03$
2004/10/09	$0.82 \pm 0.03$	$1.28 \pm 0.03$	$0.46 \pm 0.03$
2005/10/01	$0.76 \pm 0.06$	$1.18 \pm 0.06$	$0.42 \pm 0.03$
2005/11/04	$0.67 \pm 0.04$	$1.14 \pm 0.03$	$0.47 \pm 0.03$
2005/11/06	$0.70 \pm 0.03$	$1.19 \pm 0.03$	$0.48 \pm 0.03$
2006/06/29	$0.73 \pm 0.04$	$1.21 \pm 0.04$	$0.48 \pm 0.03$
2006/08/18	$0.77 \pm 0.03$	$1.23 \pm 0.03$	$0.46 \pm 0.03$
2006/08/19	$0.71 \pm 0.03$	$1.18 \pm 0.03$	$0.47 \pm 0.03$
2006/08/25	$0.61 \pm 0.04$	$1.06 \pm 0.04$	$0.45 \pm 0.03$
2006/10/23	$0.72 \pm 0.06$	$1.14 \pm 0.05$	$0.42 \pm 0.04$
2006/10/24	$0.71 \pm 0.06$	$1.27 \pm 0.06$	$0.56 \pm 0.04$
2007/09/10	$0.63 \pm 0.03$	$1.07 \pm 0.03$	$0.44 \pm 0.02$
2007/10/04	$0.65 \pm 0.02$	$1.10 \pm 0.02$	$0.45 \pm 0.02$

frame. They were selected among the most stable stars in the field (see Sec. 2.3). The results of the differential photometry are given in Table 3 and Fig. 2. The points from SAO (solid circles) are with bigger errors, because of the smaller telescope aperture and the shorter exposure times (Table 2).

### 2.3 Photometric Calibration

The absolute calibration of our instrumental magnitudes includes three steps. First, we tied the FORS1@VLT image to the Landolt (1992) standard field MARK A. Then, we searched for all stars in common between the FORS1@VLT image and eight other images from NAO Rozhen, obtained under photometric conditions until 2006 August and calculated transformations between the individual frames. Finally, using these nine images we derived new magnitudes for a few additional stars, bringing the number of reference stars in the field to 24. Here we consider only stars with  $\text{rms} \leq 0.04$  mag making sure the calibration is based only on non-variable sources (Table 4 and Fig. 3). The weights used for averaging the magnitudes were  $\sigma^{-2}$ , where:

$$\sigma = \sqrt{\sigma_{zp}^2 + \sigma_{inst}^2}. \quad (3)$$

Here  $\sigma_{zp}$  is the error of the zero-point and  $\sigma_{inst}$  is the instrumental magnitude's error. The total uncertainty is dominated by the zero-point errors with a typical value to  $\sim 0.03$  mag. The instrumental error of individual measurements attains 0.01 mag at  $R_C \sim 20.5$  mag level (Table 4).

### 2.4 Literature data and filter transformation

The observations of McCarthy et al. (1988), Schneider et al. (1989) and (Crampton et al. 1992; private communication) provided additional measurements of Q 2203+292 (Table 1). Since some of them were observed in filters other than the  $R_C$  filter used by us and we have to compare the luminosity of Q 2203+292 with the luminosities of quasars at similar

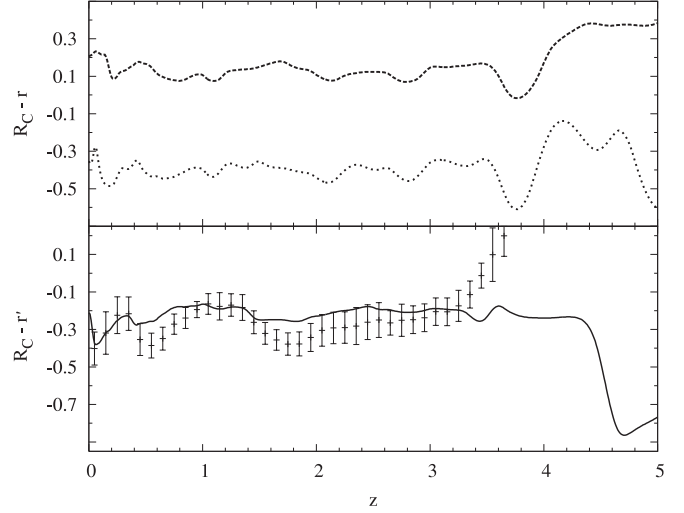
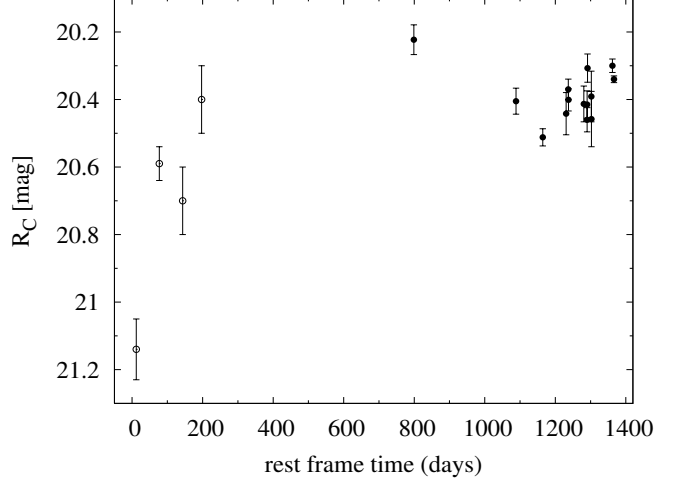
**Table 4.** Reference stars in the field of the quasar Q 2203+292. The quasar magnitude is for the 2004 October 9 image.

ID	RA (2000.0)	DEC	$R_C(\text{err})$ , mag
Q	22:06:02.70	29:30:02.0	20.51 (0.03)
A	22:06:07.15	29:30:12.9	19.69 (0.01)
B	22:06:06.33	29:31:08.0	19.23 (0.02)
1	22:06:12.17	29:28:26.0	20.29 (0.03)
2	22:06:13.47	29:28:45.3	19.43 (0.03)
3	22:06:00.42	29:29:13.7	18.58 (0.03)
4	22:06:11.51	29:29:17.9	19.40 (0.04)
5	22:05:54.95	29:29:22.6	20.23 (0.03)
6	22:06:08.80	29:29:24.1	20.03 (0.03)
7	22:05:58.62	29:29:26.2	18.60 (0.02)
8	22:06:12.79	29:29:40.8	19.03 (0.02)
9	22:05:55.39	29:29:42.9	17.72 (0.03)
10	22:05:54.13	29:29:50.9	20.26 (0.03)
11	22:05:59.95	29:29:51.6	19.96 (0.03)
12	22:05:55.51	29:29:55.0	19.99 (0.04)
13	22:05:54.92	29:29:58.5	19.88 (0.03)
14	22:05:59.73	29:30:00.8	18.61 (0.03)
15	22:06:02.24	29:30:01.1	20.45 (0.03)
16	22:06:11.07	29:30:04.1	19.67 (0.03)
17	22:06:05.93	29:30:29.0	19.91 (0.03)
18	22:05:54.04	29:31:13.9	19.19 (0.03)
19	22:05:59.18	29:31:19.4	20.18 (0.03)
20	22:05:58.68	29:31:22.7	18.80 (0.02)
21	22:05:56.55	29:31:23.1	19.08 (0.02)
22	22:06:02.73	29:31:37.0	19.24 (0.02)

redshift observed in  $r'$ , we were forced to derive transformations to the Cousins  $R_C$  system.

We calculated  $R_C - r$  for a  $z=4.4$  QSO using the Q 2203+292 spectrum from Constantin et al. (2002) convolving it with the transmission curves of the standard  $R_C$  filter and the other  $r$  filters used in the literature studies. To obtain the necessary spectral coverage, we combined it with the bluest part of the Q 2203+292 spectrum from McCarthy et al. (1988), shortwards of 1070 Å. Here and throughout this paper we used the following zero-point fluxes: 3080 Jy for  $R_C$  (Bessell 1979), 2810 Jy for  $r_s$  system (Djorgovski 1985), 4471 Jy for  $r_4$  (Frei & Gunn 1994) and 3631 Jy for  $r'$  AB system (Oke & Gunn 1983).

We also calculated  $R_C - r$  as a function of redshift  $z$  to compare our corrections with the literature, and to derive K-corrections for a comparison of the properties of Q 2203+292 and the SDSS QSOs (see Sec. 3.2). We created our own composite spectrum, combining the Constantin et al. (2002) median spectrum with the bluest part of the McCarthy et al. (1988) shortwards of 1150 Å (which contributes very little flux to any of the  $r$  filters). Finally, the reddest part of our template ( $\lambda > 1450$  Å) comes from the Vanden Berk et al. (2001). Indeed, the composite is dominated by lower redshift ( $z \leq 2$ ) quasars. The overall behavior of  $R_C - r$  as a function of  $z$  is shown in Fig. 4. The bottom panel demonstrates the agreement between our synthetic photometry and the mean  $R_C - r'$  colour for the quasars with  $r'$  photometry from the SDSS QSO sample (Schneider et al. 2005) after applying the colour equations of Jester et al. (2005; see their table 1). Although these transformations were derived for quasars with  $z < 2.1$ , the figure suggests that they can be extrapolated

**Figure 4.** The  $R_C - r$  colours versus the redshift  $z$ . The upper panel shows colour terms for  $r_s$  (dashed line) and  $r_4$  (dotted line). The bottom panel shows  $R_C - r'$  (solid line) and the behavior of the mean colour of the SDSS QSO sample according to Jester et al. (2005). The synthetic colours were derived from our composite QSO spectrum.**Figure 5.** Light curve of the quasar Q 2203+292 in the rest frame. The open circles show the literature data (Table 1) and the filled circles are our measurements.

lated even up to  $z \sim 3.3$ . For higher redshifts, Ly $\alpha$  enters the filter passband rendering them unusable.

The corrections for Q 2203+292 in  $R_C$  system are:  $R_C - r_s = +0.36$  mag,  $R_C - r_4 = -0.29$  mag. We assign to them tentative errors equal to the differences between the  $R - r$  values derived for this redshift from the quasar spectrum and from our own composite spectrum: 0.02 mag for both  $R_C - r_s$  and  $R_C - r_4$ . They were added in quadrature to the observational uncertainties of the first two data points of our light curve (Fig. 5). Table 5 lists all available photometry for Q 2203+292 in the  $R_C$  filter, including the corrected literature measurements. Note, that here we combine systematic with random errors, though.

**Table 5.** Final  $R_C$  light curve of Q 2203+292. See Sec. 2.4 for details. References: 1 McCarthy et al. (1988), 2 Schneider et al. (1989), 3 Crampton et al. (1992), 4 Crampton (private communication), 5 this work.

JD-2447000+ $R_C$ (error),mag	Ref.
0064.04166	21.14 (0.09) 1
0417.28020	20.59 (0.05) 2
0773.84030	20.70 (0.10) 3
1064.04170	20.40 (0.10) 4
4313.43375	20.22 (0.04) 5
5878.38186	20.41 (0.04) 5
6288.31451	20.51 (0.03) 5
6645.39887	20.44 (0.06) 5
6679.30514	20.37 (0.03) 5
6681.28100	20.40 (0.03) 5
6916.41181	20.41 (0.05) 5
6966.39679	20.46 (0.04) 5
6967.42921	20.42 (0.04) 5
6972.54666	20.31 (0.04) 5
7032.18690	20.39 (0.08) 5
7033.28848	20.46 (0.08) 5
7354.46565	20.30 (0.02) 5
7378.27326	20.34 (0.01) 5

### 3 DISCUSSION

#### 3.1 Variability

The quasar shows (Fig. 5) a brightness increase of  $\sim 0.75$  mag at the beginning of the coverage but it is nearly constant later. Due to the gaps in the lightcurve, any non-linear fluctuations (such as flares) cannot be ruled out. We verify the variability properties of the Q 2203+292 by means of differential photometry and Monte Carlo simulation.

The differential light curves (Fig. 2) of the quasar were generated with respect to the reference stars A and B, two of the most stable stars near the quasar. The rms of the relative light curve A–B is 0.035 mag, and since the two stars have similar magnitudes, their individual errors are  $\sim 0.025$  mag. The rms for the quasar light curve with respect to star A (marked as Q–A) is 0.083 and with respect to star B (marked as Q–B) is 0.086 mag. The maximum peak-to-peak variation of the quasar is  $\sim 0.92$  mag over the entire monitoring period (Table. 5) but it is reduced to 0.21 mag if we consider only the Rozhen observations. The rms of all 18 QSO measurements is 0.20 mag, and if only our 14 measurements are considered, it decreases to 0.08 mag.

To test further the variability of Q 2203+292, we carried out a Monte Carlo simulation drawing 18 measurements from a constant source with the measured mean magnitude of Q 2203+292. Each of these points was generated from a Gaussian distribution with the observational error of the corresponding measurement, so that the artificial datasets more faithfully represent the properties of the real observations. If we consider all data, including the ones from the literature, none of one million simulated data sets exceeded the observed rms. However, the colour transformations can be a source of extra uncertainty, so we carried the same simulation only for our 14 measurements to obtain that in 98.5 per cent of the cases the data are inconsistent with a

constant source. Excluding the VLT point lowers this probability down to 86.4 per cent.

We conclude that if the colour transformation of the historical observations can be considered reliable, the quasar have undergone a brightening episode in the past but the unaccounted systematic effects stop is from making a strong statement about this. All the literature data consistently deviate from ours in one direction, albeit by different amount, hinting that the variation may be real. Next, our own data show that during the recent years the quasar is in relatively stable state.

The  $R_C$  band in the rest-frame of the quasar correspond to the UV flux between 970 and 1420 Å, including the Ly $\alpha$  emission line. To compare the variability properties of Q 2203+292 with those of lower redshift quasars, we calculated the structure function  $S(\tau)$ , which is commonly used to characterize the variability of large quasar samples (i.e. Hughes, Aller & Aller 1992):

$$S(\tau) = \langle [m(t) - m(t + \tau)]^2 \rangle. \quad (4)$$

Here,  $m(t)$  is the magnitude at time  $t$  and  $\tau$  is the time interval between the two measurements in the QSO rest frame. The broken brackets express ensemble average over measurements with the same time interval. The structure function is less sensitive to the inhomogeneity of the observational coverage, and it can be applied to both individual objects and to samples of objects. Note that sometimes in the literature the structure function is defined as a square root of the ensemble average.

The structure function for Q 2203+292 is shown in Fig. 6. The small number of measurements that form each bin lead to large uncertainties making it difficult to draw definite conclusions. The overall shape of  $S(\tau)$  for Q 2203+292 is similar to that of other QSOs studied in the literature (i.e. Vanden Berk et al. 2004). It is dominated by observational errors for short time intervals and by the intrinsic QSO variability for the longer ones. There is indication that  $S(\tau)$  may reach a plateau at time scale just above 1 yr. However, quasars are known to vary on a much longer time-scale, so we interpret this as poor sampling. Note that the structure functions of some QSOs may show intrinsic structure in  $S(\tau)$  that is often interpreted as variability driven by more than one physical mechanism (see Hughes et al. 1992 for examples). We can not exclude that this can be the case with Q 2203+292. Further observations over longer time span are necessary to address this question.

A quick comparisons with the literature, typically for  $\tau \sim 0.5$ –2 yr, shows that Q 2203+292 is relatively more variable than the average QSO in the samples of Cristiani et al. (1996) and Wold et al. (2007) and comparable with those of di Clemente et al. (1996) and de Vries et al. (2003).

Recently, Wold et al. (2007) explored the dependence of the quasar variability from the mass of the central black hole. For  $M_{BH} = 10^8$ – $10^9 M_\odot$  – as estimated for Q 2203+292 by Turner (1991) – they obtain  $R$ -band amplitude of 0.3–0.4 mag, which is similar to the value reported here.

#### 3.2 Physical properties of Q 2203+292

To calculate the absolute luminosity of Q 2203+292, we adopted the following cosmological parameters:  $\Omega_\Lambda = 0.7$ ,  $\Omega_M = 0.3$ , and  $H_0 = 70 \text{ km s}^{-1} \text{ Mpc}^{-1}$ .



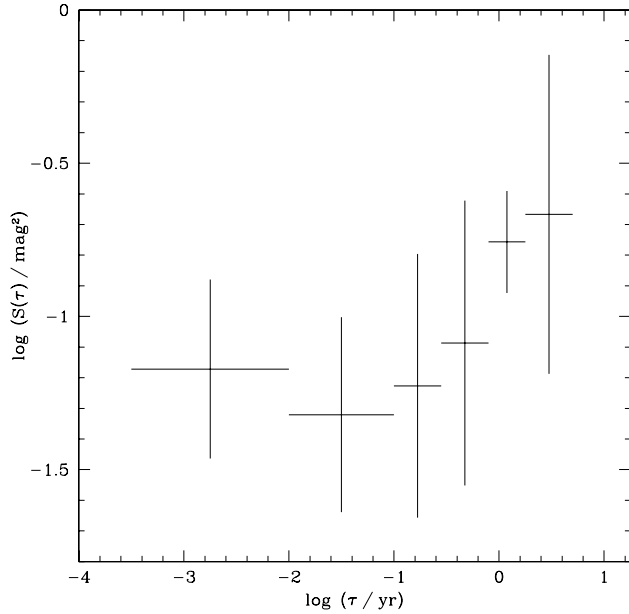


**Figure 6.**  $R$ -band structure function for the quasar Q 2203+292 in the rest frame time. The horizontal bars mark the width of the bins used in the ensemble averaging and the vertical ones are the corresponding rms

The absolute  $R$ -band magnitude,  $M_R$ , is related to the apparent magnitude,  $R$ , by

$$M_R = R - A_R - 5 \log d_L - 2.5 \log(1+z) - 25 + \Delta R_{kcorr}(z) \quad (5)$$

where  $A_R$  is Galactic absorption, and  $d_L$  is the luminosity distance for a flat Universe.

The K-correction  $\Delta R_{kcorr}(z)$  is calculated by convolving a quasar spectrum with a sensitivity curve for a standard  $R_C$  filter (Fig. 7). We used our composite spectrum (see Sec. 2.4) for the SDSS quasars observed in  $r'$  (Schneider et al. 2005) and the Q 2203+292 spectrum from Constantin et al. (2002) for our target. In the latter case  $\Delta R_{kcorr}=0.25$  mag, 0.06 mag smaller than the value derived for  $z=4.40$  from the composite spectrum. Although this is a systematic rather than random error, we added this difference in quadrature to the  $M_R$  uncertainty (equal to the rms of all Q 2203+292 measurements) to obtain a conservative error estimate. Assuming  $A_R=0.25$  mag (Schlegel, Finkbeiner & Davis 1998) and using the average  $R_C=20.46$  mag we obtained  $M_R=-29.39$  mag, typical for the SDSS quasar distribution at that redshift (Fig. 8).

The minimum mass of the emitting gas in the quasar broad line region (BLR) can be estimated following Baldwin et al. (2003), assuming Case B recombination, when all Ly $\alpha$  photons escape and the electron temperature is  $T_e=20,000$  K:

$$M_{BLR} = 5.1(10^{11}/n_e)(L_{Ly\alpha}/10^{45}) M_\odot, \quad (6)$$

where  $L_{Ly\alpha}$  is the Ly $\alpha$  luminosity and  $n_e$  is the electron density.

We measured  $L_{Ly\alpha}$  from the spectra of Schneider et al. (1989) and Constantin et al. (2002):  $8.6 \times 10^{43}$  and  $5.6 \times 10^{43}$  erg s $^{-1}$ , respectively. Naturally, these are only lower limits

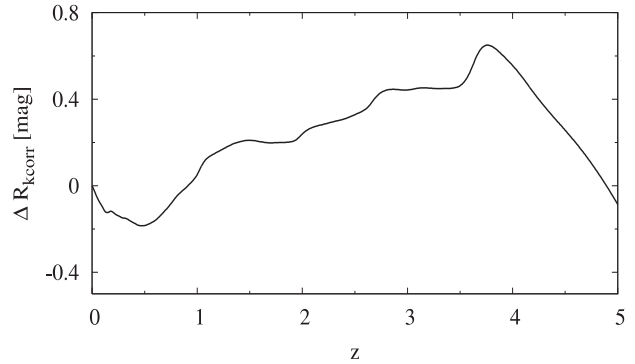


**Figure 7.**  $R_C$ -band K-correction as a function of the redshift.

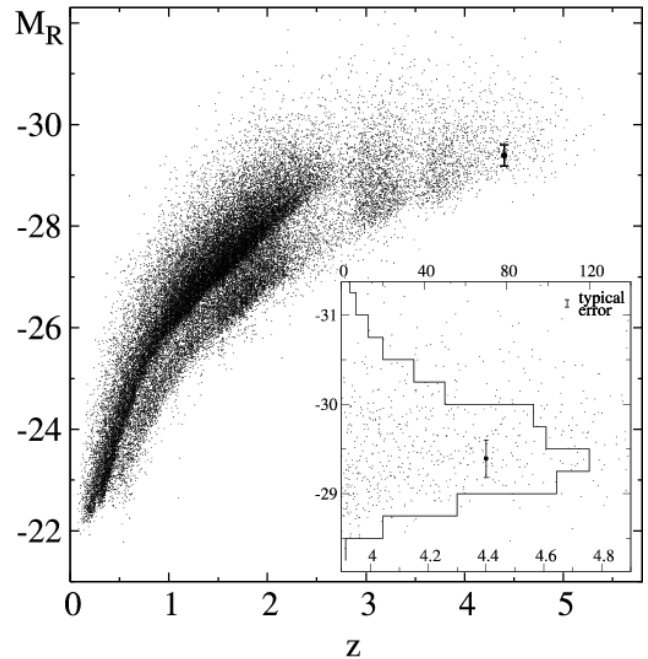


**Figure 8.** Comparison of the absolute magnitude  $M_R$  of Q 2203+292 and 46420 SDSS quasars from Schneider et al. (2005). The apparent  $R$  magnitudes of the SDSS quasars were calculated from the SDSS  $r'$  magnitudes according to the colour transformations described in Sec. 2.4 (see also Fig. 4, bottom panel). The bigger dot marks the average absolute luminosity of Q 2203+292 and the errorbars are the rms. The inset shows a histogram of  $M_R$  for 625 quasars at  $z$  between 3.9 and 4.9. Again, the location of Q 2203+292 measurement is shown with a bigger dot.

because of the Ly $\alpha$  self-absorption. In both cases, we fitted the quasar continuum with a power law  $F_\nu \propto \nu^\alpha$ , and fixing  $\alpha=-1.0$ . Assuming  $n_e=10^{11}$  cm $^{-3}$ , we obtain  $M_{BLR}=0.44$  and  $0.29 M_\odot$  for the measurements from the two spectra.

### 3.3 Miscellaneous: Search for associated emission line objects

Narrow band Ly $\alpha$  imaging down to 25.5 mag per sq. arcsec (McCarthy et al. 1988) yielded no other emission line sources at the same redshift within  $2 \times 2$  arcmin $^2$  from Q 2203+292. Thompson, Djorgovski & Beckwith (1994) failed to find as-

sociated [OIII] emitters in  $18.2 \times 19.4$  arcsec<sup>2</sup> field centred at the quasar.

We used the Photometrics AT200A camera at the 2m telescope at the Rozhen Observatory to carry out a search for associated emission line objects on 2006 August 19. The observations were obtained through a narrow band (FWHM=32 Å) interference filter *IF658* centred at 6572 Å, corresponding to Ly $\alpha$  at  $z \sim 4.4$ . Our field of view was 5 arcmin<sup>2</sup>, which is much bigger than that in the earlier studies. The exposure time was 2 h, which was split into six 1200 s exposures. We found no evidence for sources with emission lines falling into the bandpass of our narrow band filter down to a surface brightness level of  $\sim 24.5$  mag per sq. arcsec, in agreement with the previous attempts.

#### 4 SUMMARY

We carried out multi-year photometric  $R_C$ -band monitoring of the  $z=4.40$  radio quiet quasar Q 2203+292, and we found that it exhibits maximum peak-to-peak difference between two points on the light curve of  $\sim 0.3$  mag for our data and  $\sim 0.9$  mag when combined with older literature data. The rms amplitude of the lightcurve is 0.08 mag and 0.20 mag, respectively. The detected variability is at  $\sim 3\sigma$  level when the photometric accuracy of the both data sets are taken into account. The Monte Carlo simulation can not reproduce the observed variation with a constant source in 10<sup>6</sup> simulations, if we consider all the data but it does in 2.5 per cent of the simulations if we exclude the literature data and in 13.6 per cent is we consider only the Rozhen and SAO observations. These results lead us to the conclusion that during the recent years the quasar is in a stable state but we refrain from making a strong statement about the earlier variability because of possible unaccounted systematic effects in the transformation between the different photometric systems.

Unlike previous works, which used large samples of quasars to determine their variability properties, our goal was to assemble a well sampled light curve of individual quasars. The structure function analysis concluded that the object shows variability properties similar to those of the lower redshift quasars. We also found that narrow-band imaging at the redshifted Ly $\alpha$  shows no other emission line objects within  $5 \times 5$  arcmin<sup>2</sup> field.

#### 5 ACKNOWLEDGMENTS

This work was partially supported by the following grants: *VUF201/06*, *MUF04/05*, *F1302/03* of the Bulgarian Science Foundation and 008/07 with the Sofia University. The authors thank Dr. David Crampton for giving us access to unpublished data and to Dr. Anca Constantin for providing the Q 2203+292 spectrum and the median composite spectrum of high redshift quasars. We thank Dr. Haralambi Markov for his help with the spatial correction of the instrumental magnitudes, Dr. Tanyu Bonev for his assistance with the FoReRo2 observations and Dr. Ilia Roussev for editing the manuscript. We also wish to thank the anonymous referee for the useful comments that helped to improve the paper greatly.

#### REFERENCES

- Baldwin, J. A., Ferland, G. J., Korista, K. T., Hamann, F. & Dietrich, M. 2003, *ApJ*, 582, 590  
 Bessell, M. S. 1979, *PASP*, 91, 589  
 Blandford, R. D. & McKee, C. F. 1982, *ApJ*, 255, 419  
 Giveon, U., Maoz, D., Kaspi, S., Netzer, H. & Smith, P. S. 1999, *MNRAS*, 306, 637  
 Constantin, A., Shields, J. C., Hamann, F., Foltz, C. B. & Chaffee, F. H. 2002, *ApJ*, 565, 50  
 Crampton, D., McClure, R. D. & Fletcher, J. M. 1992, *ApJ*, 392, 23  
 Cristiani, S., Trentini, S., La Franca, F., Aretxaga, I., Andreani, P., Vio, R. & Gemmo, A. 1996, *A&A*, 306, 395  
 de Vries, W. H., Becker, R. H. & White, R. L. 2003, *AJ*, 126, 1217  
 de Vries, W. H., Becker, R. H., White, R. L. & Loomis, C. 2005, *AJ*, 129, 615  
 di Clemente, A., Giallongo, E., Natali, G., Trèvese, D. & Vagnetti, F. 1996, *ApJ*, 463, 466  
 Dickinson, M. & McCarthy, P. J. 1987, *BAAS*, 19, 1125  
 Dietrich, M. & Hamann, F. 2004, *ApJ*, 611, 761  
 Djorgovski S. 1985, *PASP*, 97, 1119  
 Frei, Z. & Gunn, J. E. 1994, *AJ*, 108, 1476  
 Hawkins, M. R. S. 2002, *MNRAS*, 329, 76  
 Hawkins, M. R. S. 2007, *A&A*, 462, 581  
 Hook, I. M., McMahon, R. G., Boyle, B. J. & Irwin, M. J. 1994, *MNRAS*, 268, 305  
 Hovatta T., Tornikoski M., Lainela, M., Lehto, H. J., Valtaoja, E., Tornainen, I., Aller, M. F. & Aller, H. D. 2007, *A&A*, 469, 899  
 Hughes, P. A., Aller, H. D. & Aller, M. F. 1992, *ApJ*, 396, 469  
 Jester, S. et al. 2005, *AJ*, 130, 873  
 Jockers, K. et al. 2000, *KFNTS*, 3, 13  
 Kaspi, S., Brandt, W. N., Maoz, D., Netzer, H., Schneider, D. P. & Shemmer, O. 2007, *ApJ*, 659, 997  
 Kochanek, C. S. 1993, *ApJ*, 417, 438  
 Landolt, A. U. 1992, *AJ*, 104, 340  
 Leighly, K. M., Halpern, J. P., Jenkins, E. B. & Casebeer, D. 2007, *ApJS*, 173, 1  
 Longair, M. S. & Gunn, J. E. 1975, *MNRAS*, 170, 121  
 Markov, H. 2005, *BlJPh*, 32, 1, 59  
 McCarthy, P. J., Dickinson, M., Filippenko, A. V., Spinrad, H. & van Breugel, W. J. M. 1988, *ApJ*, 328, 29  
 Nicastro, F. 2000, *ApJ*, 530, L65  
 Oke, J. B. & Gunn, J. E. 1983, *ApJ*, 266, 713  
 Omont, A., McMahon, R. G., Cox, P., Kreysa, E., Bergeron, J., Pajot, F. & Storrie-Lombardi, L. J. 1996, *A&A*, 315, 1  
 Peterson, B. M. et al. 2004, *ApJ*, 613, 682  
 Riley, J. M., Longair, M. S. & Gunn, J. E. 1980, *MNRAS*, 192, 233  
 Schlegel, D. J., Finkbeiner, D. P. & Davis, M. 1998, *ApJ*, 500, 525  
 Schmidt, M., van Gorkom, J. H., Schneider, D. P. & Gunn, J. E. 1995, *AJ*, 109, 473  
 Schneider, D. P., Schmidt, M. & Gunn, J. E. 1989, *AJ*, 98, 1507  
 Schneider, D. P., van Gorkom, J. H., Schmidt, M. & Gunn, J. E. 1992, *AJ*, 103, 1451  
 Schneider, D. P. et al., 2005 *AJ*, 130, 367  
 Shemmer, O. et al., 2006, *ApJ*, 644, 86  
 Stalin, C. S. & Srianand, R. 2005, *MNRAS*, 359, 1022  
 Stetson, P. B. 2000, *PASP*, 112, 925  
 Surdej, J. et al. 1993, *AJ*, 105, 2064  
 Thompson, D., Djorgovski, S. & Beckwith, S. V. W. 1994, *AJ*, 107, 1  
 Turner, E. L. 1991, *AJ*, 101, 5  
 Ulrich, M. H., Maraschi, L. & Urry, C. M. 1997, *ARA&A*, 35, 445  
 Vanden Berk, D. E. et al. 2001, *AJ*, 122, 549  
 Vanden Berk D. E. et al. 2004, *ApJ*, 601, 692



